Environmental Science & Technology

Article

Cite This: Environ. Sci. Technol. 2018, 52, 107−113

pubs.acs.org/est

Sequestration of Antimony on Calcite Observed by Time-Resolved Nanoscale Imaging

François Renard,*[,†,‡] Christine V. Putnis,[§,∥] German Montes-Hernandez,[‡] Helen E. King,[⊥] Gijs D. Breedveld,[†,#] and Gudny Okkenhaug[#,∇]

[†]Department of Geosciences, Physics of Geological Processes, University of Oslo, Oslo, Norway

[‡]Univ. Grenoble Alpes, CNRS, ISTerre, 38000, Grenoble, France

[§]Institut für Mineralogie, University of Münster, Corrensstrasse 24, 48149 Münster, Germany

[∥]The Institute for Geoscience Research (TIGeR), Department of Chemistry, Curtin University, Perth, 6845, Australia

[⊥]Department of Earth Sciences, Utrecht University Budapestlaan 4, 3584 CD Utrecht, The Netherlands

[#]Norwegian Geotechnical Institute, box 3930, Ullevål Stadion, 0806 Oslo, Norway

[∇]Norwegian University of Life Sciences, Faculty of Environmental Sciences and Natural Resource Management, box 5003, 1432 Ås, Norway

Supporting Information

ABSTRACT: Antimony, which has damaging effects on the human body and the ecosystem, can be released into soils, ground-, and surface waters either from ore minerals that weather in near surface environments, or due to anthropogenic releases from waste rich in antimony, a component used in batteries, electronics, ammunitions, plastics, and many other industrial applications. Here, we show that dissolved Sb can interact with calcite, a widespread carbonate mineral, through a coupled dissolution−precipitation mechanism. The process is imaged in situ, at room temperature, at the nanometer scale by using an atomic force microscope equipped with a flow-through cell. Time-resolved imaging allowed following the coupled process of calcite dissolution, nucleation of precipitates at the calcite surface and growth of these precipitates. Sb(V) forms a precipitate, whereas Sb(III) needs to be oxidized to Sb(V) before being incorporated in the new phase. Scanning-electron microscopy and Raman spectroscopy allowed identification of the precipitates as two different calcium−antimony phases ($Ca_2Sb_2O_7$). This coupled dissolution−precipitation process that occurs in a boundary layer at the calcite surface can sequester Sb as a solid phase on calcite, which has environmental implications as it may reduce the mobility of this hazardous compound in soils and groundwaters.

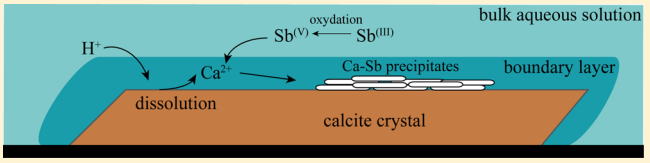

INTRODUCTION

The environmental presence and behavior of antimony (Sb), a hazardous substance as a solid or in solution, is gathering increased attention due to its increasingly extensive use in various products and its fate in the environment. The use of Sb includes applications as flame retardant in plastics, rubbers, textiles, brake pads, pigments, paints, ceramics, and semiconductor materials such as GaSb and InSb in electronic devices. In addition, it is present as a lead alloy in storage batteries and ammunitions. Substantial Sb emissions are related to mining and smelting activities and spent ammunitions at shooting ranges.[1,2] Its widespread use results in high concentrations present in waste, including air pollution control residues (i.e., ashes of flue gas treatment) from waste incineration.[3] Consequently, soils can show significant concentrations of Sb,[4,5] leading to elevated levels in soil pore water and groundwater.[5]

Antimony can be found in four oxidation states (−III, 0, III, and V), of which Sb(III) as neutral antimonite ($Sb(OH)_3$) and Sb(V) as antimonate ($Sb(OH)_6^-$) oxyanion are the most common species in natural environments.[6] In oceans, the concentration of dissolved antimony is around 0.2 $\mu g\ L^{-1}$. In nonpolluted freshwater[7] it is usually below 0.2 $\mu g\ L^{-1}$ but can sometimes reach 5 $\mu g\ L^{-1}$, while the average concentration in world rivers[6,8] is close to 1 $\mu g\ L^{-1}$. Comparatively high concentrations of up to 95 $\mu g\ L^{-1}$ antimony have been recorded in polluted groundwater and soils, where the antimony source was either natural, such as volcanic glass,[9] or anthropogenic, for example, contaminated soil and other industrial wastes.[6] Groundwater flowing out of an abandoned antimony mine near Goesdorf, Luxemburg[8] was found to contain Sb at a concentration of up to 2.2 mg L^{-1} at pH 7−8. The concentration in alkaline groundwater (pH ∼ 8) near an active mine in the Hunan province in China[10] was found to reach 11.4 mg L^{-1}; and all dissolved antimony was in the form

Received: September 13, 2017
Revised: December 5, 2017
Accepted: December 6, 2017
Published: December 6, 2017

DOI: 10.1021/acs.est.7b04727
Environ. Sci. Technol. 2018, 52, 107−113

of Sb(V). Laboratory leaching of similar mining impacted soils[1] showed water extractable concentrations of up to 748 mg kg^{-1} of soils and concentrations in water of up to 103 mg L^{-1} after 7 days contact time, for a pH range between 5 and 7.

In calcium (Ca) rich environments as calcareous soils and alkaline waste materials, Ca is suggested as an important sink for Sb. Calcium antimonates ($Ca[Sb(OH)_6]_2$ and $Ca_{1+x}Sb_2O_6OH_{2-2x}$) belong to the family of roméite minerals.[11] The solubility of roméite at room temperature[12] and pH 8 is of the order of 4 mg L^{-1}. The solubility product of romeite varies as this mineral may contain vacancies and crystallographic defects that affect dissolution.[13] Solubility between $10^{-3.4}$ and $10^{-4.8}$ mol L^{-1} at 25 °C has been proposed, with a factor 60 difference between extreme values.[13] In several industrial waste systems, the solubility product of a hydrated calcium antimonate indicates this mineral should precipitate.[14] Based on XANES spectroscopy and equilibrium calculations, it has been proposed that this mineral controls the solubility of antimony in soils near active antimony mines in China[1] or during the leaching of bottom ash from incinerated municipal waste.[14] However, to our knowledge, no direct evidence of the presence of roméite or another calcium antimony phase was provided in these studies, such as Raman spectroscopy or X-ray diffraction identification.

The dissolution−precipitation reaction of roméite at calcite interfaces could contribute to long-term spatial and temporal storage of antimony in carbonate-rich environments. The main objectives of the present study are to (1) characterize the coupling between calcite dissolution and precipitation of Ca - Sb phase(s); (2) quantify the spatial and temporal evolution of the precipitate nuclei; (3) hypothesize if a coupled dissolution−precipitation process could immobilize Sb at the calcite surface.

MATERIALS AND METHODS

A calcite crystal (Iceland spar, Vizcaya, Mexico) was obtained from the Natural History Museum in London. ICP-OES (inductively coupled plasma-optical emission spectroscopy) analyses indicate the high purity of the calcite crystal, with trace amounts of Mn (31 ppb), Mg (2.8 ppb), and Sr (11.4 ppb). Fresh calcite fragments (ca. 3 × 2 × 1 mm) were prepared directly before each experiment by cleaving the calcite crystal parallel to the {10−14} plane.

The calcite surfaces were scanned in a room with controlled temperature (22 ± 1 °C) and humidity (40%) using a Bruker Multimode Atomic Force Microscope (AFM) operating in contact mode (Supporting Information (SI)). At the beginning of each experiment, deionized water was injected over the calcite surface for several minutes, to observe any reaction or dissolution. Then, antimony-free solutions and solutions with a controlled amount of Sb (Sb(III) or Sb(V)), with the same constant ionic strength (0.05 M) and various controlled pH values between 2 and 8, were injected (SI Table S1). Several solutions with identical compositions were used to test the reproducibility of the obtained results.

The same procedure described below was followed in each experiment to ensure results could be compared between experiments. First, deionized water was injected for 10 min and 5 images were acquired. Second, a solution without Sb and at the desired constant pH was injected for another 10 min and 5 images were acquired. Third, solutions with increasing Sb concentrations were injected, with 5 images acquired at 1.5 min intervals, then the AFM tip was lifted for 10 min after which another image was acquired, then the AFM tip was lifted for 1 h and a further series of AFM images were acquired. Following this procedure, calcite dissolution was followed in the AFM for several hours. As a consequence, the injection was intermittent, with an average flow rate of 22 $\mu L \cdot s^{-1}$ and residence time between 1.5 min and several hours (SI).Then the sample was removed from the flow-through cell, left in contact with the solution for 12−20 h to allow sufficient time for reaction, and then imaged again. The same samples were used for scanning electron microscopy imaging and Raman spectroscopy characterization (SI).

RESULTS

Dissolution at Calcite Surface. The cleaved calcite {10−14} surface is characterized by the presence of steps (SI Figure S1a). Direct in situ observations showed that in contact with water and aqueous solutions the calcite surface dissolves along steps that retreat, as well as through the formation of etch pits with typical rhombohedral shapes (SI Figure S1b). Etch pit steps were typically one unit cell (3.1 Å) high, before deepening. These pits spread sideways to merge and remove successive unit-cell heights layer by layer. The average spreading rate $v_{avg} = (v_+ + v_-)/2$ was measured from etch pits spreading between two successive AFM scans. Here, v_+ and v_- are the velocities of the obtuse and acute steps of etch pits, respectively.[15] At pH below 4, the dissolution was so fast that it was not possible to measure etch pit spreading rates. At pH between 4.5 and 8, spreading rates and their standard deviation could be calculated from multiple measurements and found to fall in the range v_{avg} = 2.6 ± 1.3 to 4.1 ± 0.5 $nm \cdot s^{-1}$, a range of values previously reported for calcite.[15] No clear effect of Sb on the overall etch pit spreading rate could be observed. However, in all experiments where Sb(V) was injected, the shape of the initial rhombohedral etch pits evolved within minutes to show a rounding curve at the obtuse corner that seemed to be pinned (SI Figure S1c,d).

Formation of Precipitates. The precipitates initially formed as small "spots", with an average height of a few nanometers, just within the limits of AFM recognition under the given fluid conditions and contact mode. They were distributed at kink sites on the calcite surface (Figure 1) and showed low adhesion, as they were easily moved by the scanning AFM tip at the initial stage of precipitation. With time, they tended to localize near step edges (Figure 1) or near deep etch pits (Figure 2b) or, close to locations where dissolution was more intense. This means that dissolution sites where more calcium was released control the nucleation process of the precipitates. Initially the precipitates nucleated as individual particles with a rounded shape (SI Figure S2a). Then these particles either piled up or aggregated to form larger particle clusters (SI Figure S2b−d). They grew in size into larger rounded structured aggregates until they covered the whole calcite surface (Figure 2a). Even at this stage, they were weakly attached to the surface, as successive scans on the same area showed that fewer particles were present than in the surroundings (Figure 2a), which we interpret by the displacement of particles by the scanning AFM tip.

The shape and size of these precipitates could be measured in all experiments where they were observed and all showed that they formed patches with a more or less circular perimeter, a low height to diameter aspect ratio (SI Figure S3), and no evidence of crystallographic facets at the onset of precipitation. We have chosen to measure particles whose diameter is larger than 100 nm, the spatial resolution of the AFM technique used

DOI: 10.1021/acs.est.7b04727
Environ. Sci. Technol. 2018, 52, 107−113

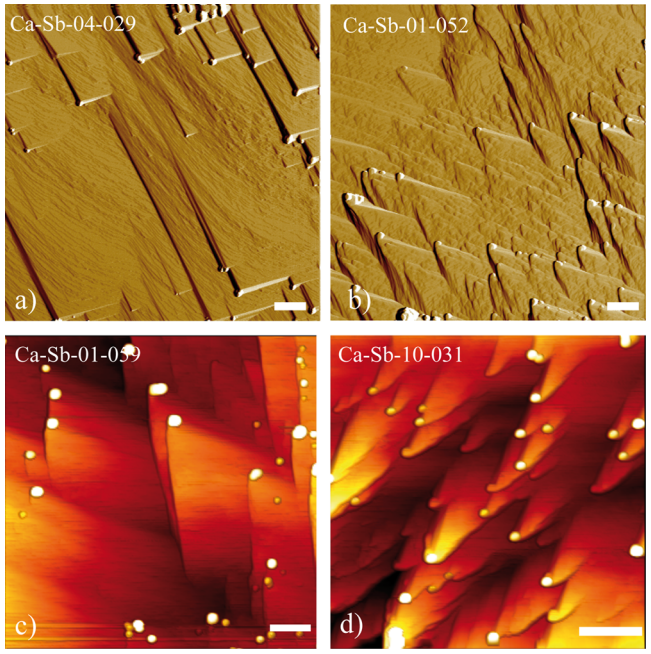

Figure 1. AFM images showing nucleation of precipitates (white spots) at step kinks on a calcite surface. (a–c) 2D images in deflection mode. (c,d) 3D rendering in height mode. Solution compositions are (a) 50 ppm of Sb(V), pH 3.2. (b,c) 200 ppm of Sb(V), pH 3; (d) 5 ppm of Sb(III), pH 3 (here probably the Sb(III) oxidized into Sb(V)). These data demonstrate that the antimony-rich precipitates nucleate near step kinks where supersaturation with respect to the new phase is also most likely. Deposits pin the steps at those points and thus inhibit dissolution locally as the steps dissolve around them, hence the appearance of the finger-like morphology emanating from these pinned points. Scale bar 1 μm.

here. With time, some of these particles developed facets (SI Figure S2d). Images were collected at different times, under different conditions, and over differing areas of observation. Under all these conditions the precipitated particles presented rounded perimeters. At the scale of the AFM observations tip-shaped convolutions would therefore be minimal. The height and diameter of the precipitates measured for all experiments (Figure 3) show that initially particles were quite flat (~10 nm), with a diameter in the range 100–200 nm. These particles formed within 2 min after the injection of Sb. With time, particles tended to grow in height, while keeping a maximum diameter smaller than 800 nm and within the range 300–800 nm. During this stage, particles aggregated or merged together and then grew in height to 20–120 nm. For three experiments the same particles could be followed in a time sequence and their height to diameter ratio showed a positive trend with time (SI Figure S3), demonstrating that particles first grew laterally (by the merging of smaller particles), as thin discs and then grew more continuously in height. In one experiment, a linear fit of the particle height with time could be performed and gives a growth rate of 0.016 nm·s^{-1} (SI Figure S4b), whereas the diameter of the precipitates did not change significantly (SI Figure S4a). .With time the calcite surface became covered by these particles that produced several layers of precipitates (Figure 2a). These observations were seen for acidic fluids in the presence of Sb; the lower the pH, the faster the calcite dissolved and more particles precipitated. Many more particles nucleated and grew in the presence of Sb(V) as compared to Sb(III).

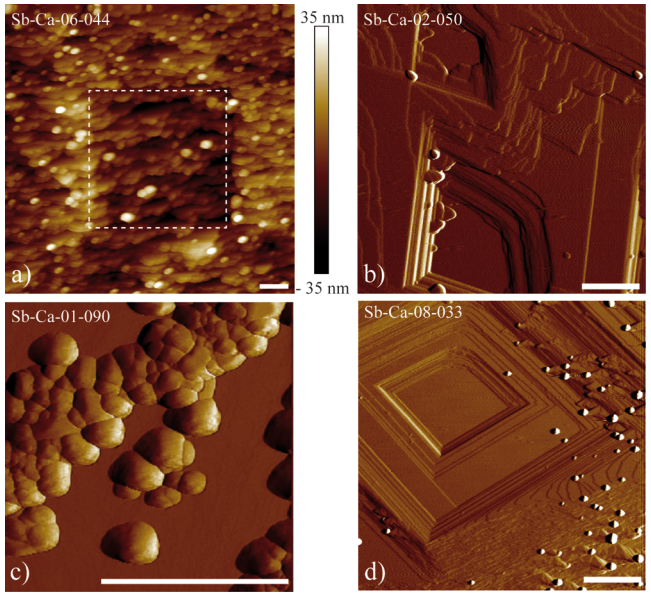

Figure 2. AFM images (deflection mode) of calcium–antimony precipitates on a calcite surface. Scale bar: 1 μm for all images. (a) Calcite surface, 10 × 10 μm^2, covered with calcium-antimonate precipitates. The central area, outlined by a dashed square, corresponds to a 5 × 5 μm^2 area scanned previously and contains less precipitates. This demonstrates that precipitates are weakly attached as some are removed by the AFM tip during scanning. Solution Sb(V) 200 ppm, pH 2.5. (b) Etch pits on calcite surface with precipitates along actively dissolving edges. The location of the precipitates is related to the location of higher dissolution. Solution Sb(V) 200 ppm, pH 5.1. (c) Image (deflection mode) of a calcite surface after 12 h in solution Sb(V) 200 ppm, pH 3 showing precipitates of calcium–antimonate that form individual patches that then agglomerate. (d) Image (deflection mode) of a calcite surface in solution Sb(III) 10 ppm pH 3, with very few precipitates of calcium-antimonate demonstrating that Sb(III) form much fewer precipitates.

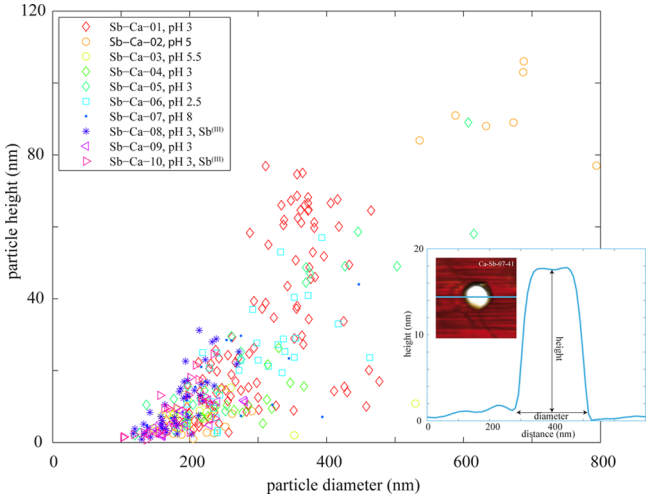

Figure 3. Height versus diameter of Ca–Sb nanoparticles in all AFM experiments. Inset: Height profile across a nanoparticle and definition of the height and diameter.

Identification of the Precipitates. Evidence for dissolution of the calcite surface and precipitation of a new phase was also observed in the SEM (Figure 4a) on calcite samples left 24 h in the Sb solutions. In the 200 ppm of Sb(V) solutions at pH 5 the calcite surface was covered in precipitates along

DOI: 10.1021/acs.est.7b04727
Environ. Sci. Technol. 2018, 52, 107–113

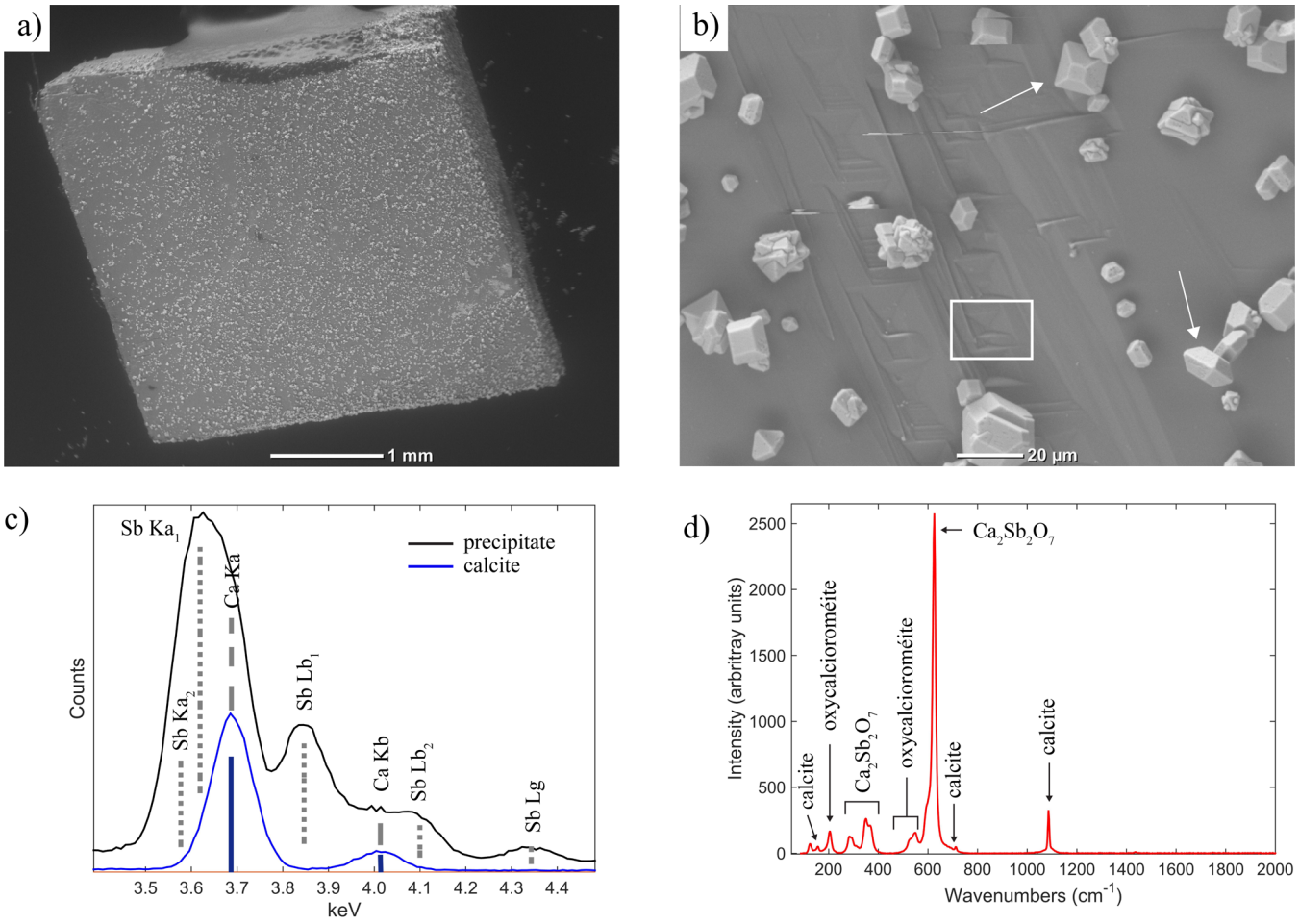

Figure 4. SEM images and EDX and Raman spectra of Ca−Sb precipitates. (a) SEM image of the calcite surface with precipitates at the surface (exp. Sb−Ca-5). (b) Higher resolution image of the precipitates showing their typical dipyramidal structures (white arrows) and the presence of etch pits on the underlying calcite surface (white box). (c) EDX spectra focused on the region between 3.4 and 4.5 eV showing the overlapping Sb, Ca peaks (blue: underlying calcite surface, gray: precipitate). (d) Typical Raman spectrum of the precipitate with phases labeled based on published spectra for oxycalcioroméite[20] and $Ca_2Sb_2O_7$ (ref 17.).

with rhombohedral etch pits seen in Figure 4b. The precipitates were between 5 and 25 μm width. These particles had clear crystal facets indicating a crystalline structure and showed a consistent dipyramidal form (Figure 4b). Incorporation of Sb into the particles was confirmed by comparison of the EDX spectra for the particles, which showed peaks for Ca Kα, Kβ, and Sb Lα Lβ in the spectral region between 3 and 5 keV, and the underlying calcite surface (Figure 4c). Raman spectroscopy of the precipitates produced spectra (Figure 4d) with peaks listed in SI Table S2. The small, sharp band at 1086 cm^{-1} is consistent with the symmetrical stretch of carbonate in the underlying calcite crystal,[16] as are the smaller peaks at 156, 283, and 711 cm^{-1}. The rest of the peaks therefore originate from the precipitate itself. The dominant peak in the spectrum at 624 cm^{-1} and the smaller peak at 384 cm^{-1} correspond well with previously published synthetic $Ca_2Sb_2O_7$ Raman spectra.[17] This mineral was also observed to form in hydrothermal experiments where calcite was left in contact with dissolved Sb.[18] However, the strong Raman peak documented for synthetic $Ca_2Sb_2O_7$ at 472 cm^{-1} is not present in the spectra obtained from the precipitates. Similarly the published spectra do not show evidence for peaks around 500 cm^{-1} that are visible in Figure 4d. This could be related to crystal orientation, which is known to change the relative intensities of peaks within the Raman spectra.[19] However, it may also be related to the precipitate chemistry or mixed phase as Raman spectra[20] from the natural mineral oxycalcioroméite ($Ca_2Sb_2O_6O$) with a more varied composition and cubic structure show dominant peaks around 500 cm^{-1}.

DISCUSSION

Dissolution−Precipitation in a Boundary Layer. The interactions of calcite with oxyanions, such as arsenic or selenium, were reported in previous studies,[21−23] where it was shown that etch pit corners could be pinned during dissolution to result in etch pit shapes deviating from normal rhombohedral etch pits, characteristic of calcite dissolving in water.[15] In the present study, a similar effect was observed, demonstrating that Sb interacts with kink sites in etch pits and slightly modify the dissolution process. However, this pinning does not have a measurable effect on the etch pit dissolution rate that remained within the average rate for calcite in pure water (2−4 $nm{\cdot}s^{-1}$).

During dissolution of calcite, ions are released such that the fluid-mineral boundary layer becomes increasingly saturated with Ca^{2+} and CO_3^{2-} ions, this last species being protonated into HCO_3^- at neutral and low pH. When the calcite surface is in contact with the Sb-bearing solution, the interfacial fluid

DOI: 10.1021/acs.est.7b04727
Environ. Sci. Technol. 2018, 52, 107−113

becomes supersaturated with a new Ca−Sb phase that can then precipitate. It is now well-established, using real-time phase-shift interferometry and ion-specific microelectrodes, that interfacial mineral-fluids can become supersaturated with a new phase when the bulk solution is undersaturated.[24] This interface-coupled dissolution−precipitation process[25,26] is summarized in the graphical abstract and involves the dissolution of the calcite substrate, releasing Ca^{2+}, followed simultaneously by the nucleation of precipitates, initially only less than 10 nm in diameter. The small rounded precipitate particles grew in diameter, until they reached a size in the range 300−800 nm, and then grew in height to 20−120 nm. Observations indicate that the initial particles merged with adjacent particles (Figures 3c; SI Figures S2b, S 2d). With time the calcite surface became covered by these particles that produced several layers of precipitates (Figure 2a). There is therefore a balance between nucleation of new precipitates and growth of existing ones.

Mechanism of Dissolution Precipitation. The interface coupled dissolution−precipitation reactions at the calcite surface can be schematically represented as follows:

$$\equiv CaCO_3 + H^+ \rightarrow Ca^{2+} + HCO_3^-$$

(dissolution process)

$$Ca^{2+} + Sb^{(V)} \rightarrow Ca - Sb^{(V)}\text{phase}$$

(precipitation process)

The appearance of tiny (few nm) particles on the dissolving calcite surface and their subsequent merging with adjacent particles tends to indicate a heterogeneous growth process that may be initiated as prenucleation clusters within the calcite-fluid boundary layer. The growth of the precipitate does not follow a classical homogeneous mechanism[27] that would require the addition of growth building ionic species to step edges and kink sites. Instead, given the limitations of our AFM observations, the first particles already with a diameter of a few nanometers appeared within seconds and at most within 1.5 min during one scan on the dissolving calcite surface. To do this, it could be assumed that some ionic species association had already occurred within the fluid boundary layer. Gebauer et al.[28] have shown that stable prenucleation ion clusters of calcium carbonate form even in undersaturated solutions. In our case the Sb-bearing solution is undersaturated with respect to any possible Ca-phase but precipitation is clearly observed on a dissolving surface. The current understanding of the mechanism of phase separation allowing for the initial formation of solid particles is an active topic of research[28] because of the application to many geochemical systems including biomineralisation. However, the formation of stable prenucleation clusters can be explained in terms of equilibrium thermodynamics that would promote some form of structural orientation between ions in solution resulting in an association of ionic species forming the initial denser cluster form. From our AFM observations it is not clear whether the initial 1−2 nm particles nucleate directly on the calcite surface or arrive at the surface already as "clusters" that have formed as prenucleation clusters within the near-surface boundary fluid layer. The latter scenario seems highly likely, given that the observations showed immediate precipitation of particles as soon as the calcite surface was in contact with a Sb-bearing solution.

The precipitation of the new phase was observed to increase with a decrease in pH, which is consistent with a faster dissolution rate of calcite at lower pH and therefore a faster release of Ca^{2+} ions required for the precipitation of the new phase. Therefore, we could reasonably expect that a Ca-antimonate phase is likely to precipitate at the calcite surface. Initially, these precipitates have a disc shape and do not show facets. With time, they develop facets (SI Figures S2d and Figure 4). $Ca_2Sb_2O_7$ has an orthorhombic crystal structure similar to weberite (Na_2MgAlF_7),[29] and often forms with a dipyramidal habit unlike oxycalcioroméite, which is isometric. Therefore, the formation of dipyramids in combination with the dominant Raman band at 624 cm^{-1} indicates that the precipitated phase is dominantly orthorhombic $Ca_2Sb_2O_7$. However, additional bands at 500 cm^{-1} in the Raman spectrum indicate some of the isometric phase is also present in the precipitates. The structure of the Ca-antimonate has been shown to be sensitive to the presence of ions such as F^-, where increase in these ions within the crystal structure encourages the formation of the isometric rather than the orthorhombic form.[30] Whether the mixed phase is due to a phase transformation during or after the experiment is unclear from the ex-situ data. As Sb-rich fluid is injected in the AFM flow-through cell, the release of Ca ions at the calcite surface, will be more concentrated near active dissolution sites such as at the bottom of etch pits or kinks. Here precipitates are initially more numerous (Figures 1 and 2b). At these locations, the concentration products of $Ca_2Sb_2O_7$, and probably oxycalcioroméite, are large enough to reach supersaturation with respect to these minerals and result in their subsequent precipitation. The precipitates grow initially as disc-shaped particles; that agglomerate into larger particles, evolving toward fully crystallized $Ca_2Sb_2O_7$ and oxycalcioroméite crystals. Such a coupled dissolution−precipitation process on carbonates has also been reported for the precipitation of a Ca arsenate phase on calcite[23] and the formation of a Ca-selenate phase on calcite.[22] These examples provide a mechanism of possible sequestration of environmentally harmful elements. More generally, such coupled replacement reactions are widespread in mineral-water systems[31] whenever the release of ions from the dissolving mineral is coupled to the precipitation of a new phase at the surface of a dissolving mineral.

Environmental Implications. The present results show that coupled to calcite dissolution, Ca−Sb phases precipitate as nanometer size particles on the calcite surface (heterogeneous nucleation). Primary nanoparticles are then self-assembled into rounded aggregates that coalesce to form larger particle aggregates averaging 130−220 nm wide and up to 80 nm high that cover the carbonate surface. There are much fewer particles at high (8) than low (2.5) pH and fewer particles in the presence of Sb(III) than in the presence of Sb(V). As confirmed by Raman spectroscopy, these particles are predominately $Ca_2Sb_2O_7$ (and probably minor oxycalcioroméite). Furthermore, we could not find any evidence for the formation of the hydrated romeite crystalline salt $Ca[Sb(OH)_6]_2$, that has been suggested to explain unexpectedly low Sb concentrations in extracts of alkaline soils.[1,12,32] This phase may possibly form at higher pH values that could be consistent with groundwater in alkaline soils. If this phase was present in the experiments, it could not be detected in the Raman data.

As a consequence of the interaction of calcite surfaces with Sb-bearing solutions, antimonate can be sequestered in a solid form on calcite surfaces by a coupled dissolution−precipitation

DOI: 10.1021/acs.est.7b04727
Environ. Sci. Technol. 2018, 52, 107−113

process in a boundary fluid layer. These results provide a mechanistic understanding of environmental studies where a Ca-antimonate phase was proposed to form, but could not previously be observed in situ.[1,4,12] Therefore, it is reasonable to suggest that calcite or other soluble Ca-bearing surfaces could provide a realistic environmental remediation strategy in the case of elevated Sb concentrations related to acid mine drainage systems, contaminated shooting range soil and ashes from waste incineration.

■ ASSOCIATED CONTENT

Supporting Information

The Supporting Information is available free of charge on the ACS Publications website at DOI: 10.1021/acs.est.7b04727.

Text (Experimental conditions), Figure S1; Figure S2; Figure S3; Table S1; and Table S2 (PDF)

■ AUTHOR INFORMATION

Corresponding Author

*E-mail: francois.renard@geo.uio.no.

ORCID

François Renard: 0000-0002-5125-5930

Helen E. King: 0000-0002-1825-782X

Author Contributions

C.V.P. and F.R. performed the experiments and wrote the manuscript. H.K. acquired and interpreted the Raman and SEM data. G.M.H., G.B., and G.O. participated to the interpretations of the experimental data and their consequences for the environment. All authors have given approval to the final version of the manuscript.

Notes

The authors declare no competing financial interest.

■ ACKNOWLEDGMENTS

We thank V. Rapelius for help with ICP-OES analyses at Münster University. C.V.P. acknowledges funding through the Marie Curie ITN CO2React. Funding from Labex OSUG@2020 (Investissement d'avenir-ANR10-LABX56) is acknowledged.

■ REFERENCES

(1) Okkenhaug, G.; Zhu, Y. G.; Luo, L.; Lei, M.; Li, X.; Mulder, J. Distribution, speciation and availability of antimony (Sb) in soils and terrestrial plants from an active Sb mining area. *Environ. Pollut.* **2011**, *159* (10), 2427−2434.

(2) Stromseng, A. E.; Ljones, M.; Bakka, L.; Mariussen, E. Episodic discharge of lead, copper and antimony from a Norwegian small arm shooting range. *J. Environ. Monit.* **2009**, *11* (6), 1259−1267.

(3) Okkenhaug, G.; Almås, Å. R.; Morin, N.; Hale; Arp, S. E.; P. H, H. The presence and leachability of antimony in different wastes and waste handling facilities in Norway. *Environmental Science: Processes Impacts* **2015**, *17* (11), 1880−1891.

(4) Scheinost, A. C.; Rossberg, A.; Vantelon, D.; Xifra, I.; Kretzschmar, R.; Leuz, A. K.; Funke, H.; Johnson, C. A. Quantitative antimony speciation in shooting-range soils by EXAFS spectroscopy. *Geochim. Cosmochim. Acta* **2006**, *70* (13), 3299−3312.

(5) Okkenhaug, G.; Gebhardt, K. A. G.; Amstaetter, K.; Bue, H. L.; Herzel, H.; Mariussen, E.; Almås, A. R.; Cornelissen, G.; Breedveld, G. D.; Rasmussen, G.; Mulder, J. Antimony (Sb) and lead (Pb) in contaminated shooting range soils: Sb and Pb mobility and immobilization by iron based sorbents, a field study. *J. Hazard. Mater.* **2016**, *307*, 336−343.

(6) Filella, M.; Belzile, N.; Chen, Y. W. Antimony in the environment: a review focused on natural waters: I. Occurrence. *Earth-Sci. Rev.* **2002a**, *57* (1), 125−176.

(7) Leyva, A. G.; Marrero, J.; Smichowski, P.; Cicerone, D. Sorption of antimony onto hydroxyapatite. *Environ. Sci. Technol.* **2001**, *35* (18), 3669−3675.

(8) Filella, M.; Belzile, N.; Chen, Y. W. Antimony in the environment: a review focused on natural waters: II. Relevant solution chemistry. *Earth-Sci. Rev.* **2002b**, *59* (1), 265−285.

(9) Nicolli, H. B.; Suriano, J. M.; Peral, Gomez; M, A.; Ferpozzi, L. H.; Baleani, O. A. Groundwater contamination with arsenic and other trace elements in an area of the Pampa, Province of Córdoba. *Environ. Geol.* **1989**, *14* (1), 3−16.

(10) Liu, F.; Le, X. C.; McKnight-Whitford, A.; Xia, Y.; Wu, F.; Elswick, E.; Johnson, C.; Zhu, C. Antimony speciation and contamination of waters in the Xikuangshan antimony mining and smelting area, China. *Environ. Geochem. Health* **2010**, *32* (5), 401−413.

(11) Brugger, J.; Gieré, R.; Graeser, S.; Meisser, N. The crystal chemistry of roméite. *Contrib. Mineral. Petrol.* **1997**, *127* (1−2), 136−146.

(12) Johnson, C. A.; Moench, H.; Wersin, P.; Kugler, P.; Wenger, C. Solubility of antimony and other elements in samples taken from shooting ranges. *Journal of Environmental Quality* **2005**, *34* (1), 248−254.

(13) Cornelis, G.; Van Gerven, T.; Snellings, R.; Verbinnen, B.; Elsen, J.; Vandecasteele, C. Stability of pyrochlores in alkaline matrices: Solubility of calcium antimonate. *Appl. Geochem.* **2011**, *26*, 809−817.

(14) Cornelis, G.; Johnson, C. A.; Van Gerven, T.; Vandecasteele, C. Leaching mechanisms of oxyanionic metalloid and metal species in alkaline solid wastes: a review. *Appl. Geochem.* **2008**, *23* (5), 955−976.

(15) Ruiz-Agudo, E.; Putnis, C. V. Direct observations of mineral-fluid reactions using atomic force microscopy: the specific example of calcite. *Mineral. Mag.* **2012**, *76*, 227−253.

(16) Edwards, H. G. M.; Villar, S. E. J.; Jehlicka, J.; Munshi, T. FT-Raman spectroscopic study of calcium-rich and magnesium-rich carbonate minerals. *Spectrochim. Acta, Part A* **2005**, *61*, 2273−2280.

(17) Gedzeciviute, V.; Welter, N.; Schüssler, U.; Weiss, C. Chemical composition and colouring agents of Roman mosaic and millefiori glass, studied by electron microprobe analysis and Raman micro-spectroscopy. *Archaeological and Anthropological Sciences* **2009**, *1*, 15−29.

(18) Itukara, T.; Sasai, R.; Itoh, H. Detoxification of antimonic contaminated water and precipitation recovery of antimony by mineralization under hydrothermal condition. *Chem. Lett.* **2007**, *36*, 524−525.

(19) King, H. E.; Mattner, D. C.; Plümper, O.; Geisler, T.; Putnis, A. Forming cohesive calcium oxalate layers on marble surfaces for stone conservation. *Cryst. Growth Des.* **2014**, *14*, 3910−3917.

(20) Biagioni, C.; Orlandi, P.; Nestola, F.; Bianchin, S. Oxy-calciooromeite, $Ca_2Sb_2O_6O$, from Buca della Vena mine, Apuan Alps, Tuscany, Italy: a new member of the pyrochlore supergroup. *Mineral. Mag.* **2013**, *77*, 3027−3038.

(21) Renard, F.; Montes-Hernandez, G.; Ruiz-Agudo, E.; Putnis, C. V. Selenium incorporation into calcite and its effect on crystal growth: An atomic force microscopy study. *Chem. Geol.* **2013**, *340*, 151−161.

(22) Putnis, C. V.; Renard, F.; King, H.; Montes-Hernandez, G.; Ruiz-Agudo, E. Sequestration of selenium on calcite surfaces revealed by nanoscale imaging. *Environ. Sci. Technol.* **2013**, *47*, 13469−13476.

(23) Renard, F.; Putnis, C. V.; Montes-Hernandez, G.; Ruiz-Agudo, E.; Hovelmann, J.; Sarret, G. Interactions of arsenic with calcite surfaces revealed by in-situ nanoscale imaging. *Geochim. Cosmochim. Acta* **2015**, *159*, 61−79.

(24) Ruiz-Agudo, E.; King, H. E.; Patiño-López, L. D.; Putnis, C. V.; Geisler, T.; Rodriguez-Navarro, C.; Putnis, A. Control of silicate weathering by interface-coupled dissolution-precipitation processes at the mineral-solution interface. *Geology* **2016**, *44* (7), 567−570.

(25) Putnis, A.; Putnis, C. V. The mechanism of reequilibration of solids in the presence of a fluid phase. *J. Solid State Chem.* **2007**, *180* (5), 1783−1786.
(26) Putnis, A. Mineral replacement reactions. *Rev. Mineral. Geochem.* **2009**, *70* (1), 87−124.
(27) Teng, H. H. How ions and molecules organize to form crystals. The mineral-water interface. *Elements* **2013**, *9*, 189−194.
(28) Gebauer, D.; Kellermeier, M.; Gale, J. D.; Bergström, L.; Cölfen, H. Pre-nucleation clusters as solute precursors in crystallization. *Chem. Soc. Rev.* **2014**, *43*, 2348−2371.
(29) Chelazzi, L.; Borrini, D.; Bonazzi, P. $Ca_2Sb_2O_7$−$Ca_3Mn^{2+}Sb_4^{5+}O_{14}$ pseudo-binary system: Synthesis and characterization by X-ray powder diffraction. *Solid State Sci.* **2011**, *13*, 195−197.
(30) Aia, M. A.; Mooney, R. W.; Hoffman, C. W. W. An X-Ray Study of pyrochlore Fluoantimonates of calcium, cadmium, and manganese. *J. Electrochem. Soc.* **1963**, *110*, 1048−1054.
(31) Putnis, A. Mineral replacement reactions: from macroscopic observations to microscopic mechanisms. *Mineral. Mag.* **2002**, *66* (5), 689−708.
(32) Oorts, K.; Smolders, E.; Degryse, F.; Buekers, J.; Gascó, G.; Cornelis, G.; Mertens, J. Solubility and toxicity of antimony trioxide (Sb_2O_3) in soil. *Environ. Sci. Technol.* **2008**, *42*, 4378.

DOI: 10.1021/acs.est.7b04727
Environ. Sci. Technol. 2018, 52, 107−113